NUMERICAL AND EXPERIMENTAL INVESTIGATION ON THE EFFECT OF RESTRICTION SHAPE ON CHARACTERISTICS OF AIRFLOW IN A SQUARE DUCT

Dr. Khalid A. H. Ismael   Dr. Ikhlase M. Fayed   Lec. Dr Hanaa Abdul Hadi

الخلاصة:

تم عرض دراسة عملية و نظرية لجريان هوائي ثلاثي الابعاد، كامل التطور ، مضطرب خلال مجرى رباعي المقطع يحتوي على عوائق بأشكال و مواقع مختلفة و لمدى رينولدز يتراوح من $8.2x10^4$ الى $5.6x10^4$. الجانب النظري للمسألة يتضمن حل المعادلات التفاضلية الجزئية الاهليليجية المتمثلة بحفظ الكتلة، الزخم ، الطاقة المضطربة و معدل ضياعها بأستخدام الحجوم المحدد (Finite Volume) . لقد حُلت هذه المعادلات سوية مع الصيغة الجبرية للزوجة المضطربة (Turbulent viscousity) بأستخدام نمـوذج (k-ε) ، بالاضافة الى أستخدام مفهوم دالة الجدار بالقرب من الجدران لمعالجـة تأثرات الاضطراب. في التجـارب العمليـة تم بناء مجرى من مادة (Perspex) علاوة على استخدام مسبار الضغط الخماسي الفتحات لقياس مركبـات السرعة الثلاثة في الحيز (مقداراً و اتجاهاً). النتائج بينت ان خسارة الضغط الكلي تعتمد على شكل و موقع العائق، و ان معامل خسارة الضغط الذي يعتمد على شكل و موقع العـائق (k_R) يعتمد على عـاملين همـا نسبة الانسداد في المساحة (A_b) ، و النسبة بين المحيط المبلل بالهواء الى المحيط الحر المتبقي (p_e/P_e)، وان هذا المعامل لا يعتمد على عدد رينولدز(لنفس نسبة مساحة الانسداد اذا ازداد p_e/P_e بنسبة 40% فان نسبة الزيادة في المعامل k_R تكون 7% ، و لنفس p_e/P_e اذا زادت نسبة مساحة الانسداد الى 50% فان نسبة الزيادة في المعامل(k_R) تكون 10% . و لكن معامل خسارة الضغط نتيجة الاحتكاك (C_f) فأنه دالة لعدد رينولدز.

ABSTRACT :

Experimental and numerical investigation has been under taken to study turbulent flow of air through duct using restriction in different shapes and positions for Reynolds numbers ranges of $(8.2x10^4 \rightarrow 5.6x10^4)$. The numerical approach used in this work is the finite volume method for solution of elliptic partial differential equation for the modeling of turbulent (k-ε) model as well as wall function concept near the wall which was used to take the turbulent effects into consideration have been employed. The experimental test rigs were constructed from Perspex, and a five-hole pressure probe was used to measure the three component of air flow velocity vector in space. The results show that the total pressure drop depends on the shape and position of the restriction, and the pressure drop coefficient due to the restriction shape and position (k_R) depends on two parameters; blockage area ratio (A_b) and the ratio between wetted perimeter to the free remainder perimeter (p_e/P_e) and dose not depend on the Reynolds number (for the same blockage area ratio A_b if the p_e/P_e increases 40%, the coefficient k_R increases 7% , and for the same $p_e/P_{e,}$ if the blockage area ratio increases 50% ,the coefficient k_R increases 10%). But the pressure drop coefficient due to the friction (C_f) is a function of Reynolds.

K. A. H. Ismael	Numerical and Experimental Investigation on the
I.M. Fayed	Effect of Restriction Shape on Characteristics of
H.A. Hadi	Airflow in a Square Duct

INTRODUCTION :

Configuration involving arrangements of sequential baffles (ribs, thin obstacles, etc.) attached to a wall are commonly used for supporting and mixing purposes in heat exchangers, nuclear reactor cores , air-cooled turbine blades, wastewater aeration tanks as wall as chemical mixers and other chemical engineering application .

Geometric parameters such as channel aspect ratio, rib to height to passage hydraulic diameter or blockage ratio, rib angle of attack, the manner in which the ribs are positioned relative to one another (in-line, staggered, crisscross, etc.), rib pitch-to-height ratio and rib shape (round versus shape corners, fillet and rib aspect ratio have pronounced effect on flow and heat transfer some of there effects have been studied in experimental and numerical research. Examples of [Han et al. (1978)], [Han (1984)],[lee (1986)],[Taslim and spring (1998)], [son et al. (2002)]. Most of the reported computational efforts [Ooi at al. 2002 & Ooi et.al (2003)] investigated the turbulent flow and heat transfer in duct with ribs using eddy viscosity type turbulence model. However, it is well known that such models are unsuitable for situation that is flow separation in the flow field. [Rasie and Bohasani (2003)] have employed low Re-k-ε turbulence model to investigation flow and heat transfer in passage with attached ribs. In this paper turbulent flow induct with restriction is numerically and experimentally investigated. The main objective of this research is to study the effect of restriction shape and position on the fluid flow characteristics in square duct for fully developed turbulent flow with different Reynolds number.

EXPERIMENTAL FACILITIES:

A centrifugal fan driven by a 550 W, 2200 r.p.m is used to supply the flow of air. The air passes through a duct (150x80 mm cross section and 600 mm length) equipped orifice meter(designed on B.S 1042) to measure flow rates and settling chamber (air box) with honeycomb at the outlet of air box.

The air box rated the air through transparency Perspex square duct (120x120 mm) with sufficient length of (1000mm) for pressure recovery represent the first part of the test section

The second part of test section is also square duct of the same dimensions (120x120x1000 mm) and material (Perspex) of the first part. At the end of the test section, the air was exhausted into the atmosphere. The connection between first and second duct were made in such manner to allow the restriction to be changed. Thirteen restriction of different shape are made from a thin galvanized sheet (1mm) as shown in Fig. (1), five-hole probe is used to measure velocity vector in the flow field down stream of restriction. To determine the magnitude and orientation of the flow vector, the surface pressure is sampled at five locations: on the axis of probe and at four equispaced points on a line encircling this central point. The pressure differentials between selected pairs of these points related to the in flow velocity vector by doing an appropriate calibration to deduce pitch and yaw directions [Hanaa (2006)]

The second duct has (48) static pressure taps on its surface (four section in z-direction of (20, 40, 80,120mm) from the test section with 12th static taps on each section with (3) taps on each surface) as shown in Fig. (2a) all static holes have a diameter of 1 mm. The section duct has four slots in the side surface which are used in the measurement by five hole probe in the four sections (20, 40, 80,120mm), Fig.(2b)

To calculate the average velocity of free stream, the inclined micro manometer is used to measure the different between the total pressure which has been measured

by pitot-tube and static pressure in front of restriction. Correction of the reading of the pitot-tube has been done according to [British standard 1042 (1973)].

The average inlet velocity for all experiments, at entrance region is (7-10 m/s) corresponding to the Reynolds number based on the hydraulic diameter (120mm) of inlet region $(5.6 \times 10^4 - 8.2 \times 10^4)$. The static pressure distributions after restriction in each section (20, 40, 80,120mm) are measured from 12th taps, so that the average pressure (P_{av}) in each can be calculated from:

$$P_{avs} = \frac{P_{s1} + P_{s2} + P_{s3} + ... + P_{s12}}{12} \tag{1}$$

to calculate the static pressure coefficient due to the friction(C_f) from:

$$C_f = \frac{P_s - P_{avs}}{1/2 \ \rho U_{av}^2}$$

where P_s static pressure before restriction.

NUMERICAL WORK:

To analyze the flow field after restriction, governing partial differential equations (conservation of mass and momentum) in three dimensions have been used. To demonstrate the effect of the turbulence on the flow, turbulence model (k-ε) is used.

It is impossible to obtain analytical solution of the partial differential equations, so numerical solution using finite volume will be done for three selection restrictions with different blockage area as shown in Fig.(3), at two Reynolds numbers $(8.2 \times 10^4$ and $5.6 \times 10^4)$. Assumption about the fluid are Newtonian, Incompressible three dimensional, turbulent flow.

(i) Continuity equation:

$$\frac{\partial U}{\partial x} + \frac{\partial V}{\partial y} + \frac{\partial W}{\partial z} = 0 \tag{2}$$

(ii) Momentum Equations:

$$\frac{\partial U^2}{\partial x} + \frac{\partial UV}{\partial y} + \frac{\partial UW}{\partial z} = -\frac{1}{\rho}\frac{\partial P}{\partial x} + \frac{\partial}{\partial x}\left(v_e \frac{\partial U}{\partial x}\right) + \frac{\partial}{\partial y}\left(v_e \frac{\partial U}{\partial y}\right) + \frac{\partial}{\partial z}\left(v_e \frac{\partial U}{\partial z}\right)$$
$$+ \frac{\partial}{\partial x}\left(v_e \frac{\partial U}{\partial x}\right) + \frac{\partial}{\partial y}\left(v_e \frac{\partial V}{\partial x}\right) + \frac{\partial}{\partial z}\left(v_e \frac{\partial W}{\partial x}\right) \tag{3}$$

$$\frac{\partial UV}{\partial x} + \frac{\partial V^2}{\partial y} + \frac{\partial UW}{\partial z} = -\frac{1}{\rho}\frac{\partial P}{\partial y} + \frac{\partial}{\partial x}\left(v_e \frac{\partial V}{\partial x}\right) + \frac{\partial}{\partial y}\left(v_e \frac{\partial V}{\partial y}\right) + \frac{\partial}{\partial z}\left(v_e \frac{\partial V}{\partial z}\right)$$
$$+ \frac{\partial}{\partial x}\left(v_e \frac{\partial U}{\partial y}\right) + \frac{\partial}{\partial y}\left(v_e \frac{\partial V}{\partial y}\right) + \frac{\partial}{\partial z}\left(v_e \frac{\partial W}{\partial y}\right) \tag{4}$$

$$\frac{\partial UW}{\partial x} + \frac{\partial VW}{\partial y} + \frac{\partial W^2}{\partial z} = -\frac{1}{\rho}\frac{\partial P}{\partial z} + \frac{\partial}{\partial x}\left(v_e \frac{\partial W}{\partial x}\right) + \frac{\partial}{\partial y}\left(v_e \frac{\partial W}{\partial y}\right) + \frac{\partial}{\partial z}\left(v_e \frac{\partial W}{\partial z}\right)$$
$$+ \frac{\partial}{\partial x}\left(v_e \frac{\partial U}{\partial z}\right) + \frac{\partial}{\partial y}\left(v_e \frac{\partial V}{\partial z}\right) + \frac{\partial}{\partial z}\left(v_e \frac{\partial W}{\partial z}\right) \tag{5}$$

Standard k-ε Model [Launder and Spalding]

$$\frac{\partial}{\partial x}(kU) + \frac{\partial}{\partial y}(kV) + \frac{\partial}{\partial z}(kW) = \frac{\partial}{\partial x}\left(\frac{v_t}{\sigma_k}\frac{\partial k}{\partial x}\right) + \frac{\partial}{\partial y}\left(\frac{v_t}{\sigma_k}\frac{\partial k}{\partial y}\right) + \frac{\partial}{\partial z}\left(\frac{v_t}{\sigma_k}\frac{\partial k}{\partial z}\right) + G - \varepsilon \tag{6}$$

$$\frac{\partial}{\partial x}(\varepsilon U) + \frac{\partial}{\partial y}(\varepsilon V) + \frac{\partial}{\partial z}(\varepsilon W) = \frac{\partial}{\partial x}\left(\frac{v_t}{\sigma_\varepsilon}\frac{\partial \varepsilon}{\partial x}\right) + \frac{\partial}{\partial y}\left(\frac{v_t}{\sigma_\varepsilon}\frac{\partial \varepsilon}{\partial y}\right) + \frac{\partial}{\partial z}\left(\frac{v_t}{\sigma_\varepsilon}\frac{\partial \varepsilon}{\partial z}\right) + C_{1\varepsilon}\frac{\varepsilon}{k}G - C_{2\varepsilon}\frac{\varepsilon^2}{k} \tag{7}$$

K. A. H. Ismael	Numerical and Experimental Investigation on the
I.M. Fayed	Effect of Restriction Shape on Characteristics of
H.A. Hadi	**Airflow in a Square Duct**

$$G = v_i \left[2\left(\frac{\partial U}{\partial x}\right)^2 + 2\left(\frac{\partial V}{\partial y}\right)^2 + 2\left(\frac{\partial W}{\partial z}\right)^2 + \left(\frac{\partial V}{\partial y}\frac{\partial U}{\partial x}\right) + \left(\frac{\partial V}{\partial z}\frac{\partial W}{\partial x}\right) + \left(\frac{\partial V}{\partial z}\frac{\partial V}{\partial y}\right) \right] \tag{8}$$

where $v_t = C\mu \dfrac{k^2}{\varepsilon}$

ε, is the dissipation term.

The empirical constants appearing in the above equations that are achieved at by comprehensive fitting data for a wide range of turbulent flows are expressed as follows:

Table (1) Empirical constants in the k-ε

C_μ	$C_{1\varepsilon}$	$C_{2\varepsilon}$	σ_k	σ_ε
0.09	*1.44*	*1.92*	*1.00*	*1.30*

BOUNDARY CONDITION:
Boundary Condition at Inlet Duct:
$U(x,y,0)= U_{in}$; $V(x,y,0)= W(x,y,0)=0$

The distribution of the inlet velocity(U_{in})can be interpolated from experimental data(7,10)m/s.

The kinetic and dissipation energy at inlet may be estimated from the following equation [Davidson and Farhanich (1995)] :

$k(x,y,0) = k_{in} = C_k\, U_{in}^2$; $\varepsilon(x,y,0) = \varepsilon_{in} = C\mu\, k_{in}^{3/2}/ (0.5 D_h C_\varepsilon)$

where (C_k, C_ε) are constant (C_k=0.003 and C_ε=0.03), while (D_h) represents hydraulic diameter of duct and its value is equal to the section length of the square duct.

Boundary Condition at the Wall:
For no slip ($U=V=W=0$) is the appropriate condition for the velocity component at solid walls [Verstage and Malasekera (1995)]. Due to the viscous influence near wall, the local Reynolds number becomes very small, thus the turbulent modal which is designed for high Reynolds number become inadequate. In this case, the calculation of shear stress near the wall needs a special treatment. In order to adequately avoid these problems, it would be necessary to employ a fine grid near the wall, which would be expensive. An alternative and widely employed approach is to use formula which known as "wall function".

THE GENERAL FORM OF THE GOVERING (PDES):
The general partial differential equations (i.e. sometimes called transport equations) [Patanker (1980)] for continuity, momentum scales k,ε all have the form

$$\frac{\partial}{\partial x}(\rho U\phi) + \frac{\partial}{\partial y}(\rho V\phi) + \frac{\partial}{\partial z}(\rho W\phi) = \frac{\partial}{\partial x}\left(\Gamma_\phi \frac{\partial\phi}{\partial x}\right) + \frac{\partial}{\partial y}\left(\Gamma_\phi \frac{\partial\phi}{\partial y}\right) + \frac{\partial}{\partial z}\left(\Gamma_\phi \frac{\partial\phi}{\partial z}\right) + S_\phi \tag{9}$$

where the three terms on the left side are convection terms and the four terms on the right side are diffusion and source term.

THREE DIMENSIONAL DISCRETIZATION:
The general transport equation may be written as:

$$\frac{\partial}{\partial x_i}(J_i) = S_\phi \tag{10}$$

Where

$$J_i = \rho U_i \phi - \Gamma_\phi \frac{\partial \phi}{\partial x_i} \qquad (11)$$

Ji represents all the flux due to both diffusion and convection. The source term may be expressed as a linear expression.

$$S_\phi = b\phi_p + c \qquad (12)$$

The pressure term is excluded from the source term (in the momentum equation) in the solution procedure, and the linearization is done for all other terms only. Integration using the CV results in:

$$J_e - J_w + J_n - J_s + J_f - J_b = (b\phi_p + c)\Delta v \qquad (13)$$

where e (east), w (west) ,n (north) and s (south) are the neighboring points of p in the y-direction, f(front), b (back) are the neighboring pointes of p in the z-direction, $\Delta v = \Delta x \Delta y \Delta z$ is the volume of the control volume. Integrating the continuity gives

$$F_e - F_w + F_n - F_s + F_f - F_b = 0 \qquad (14)$$

where the F's are the mass flow rates through the control surface. The general three-dimensional discretization equation is given by,

$$\left(\sum_i a_i - b \right)\phi_p = \sum_i a_i \phi_i + c \qquad (15)$$

where $\quad \sum_i a_i = a_p = a_E + a_W + a_N + a_S + a_F + a_B$

$$\sum_i a_i \phi_i = a_E \phi_E + a_W \phi_W + a_N \phi_N + a_S \phi_S + a_F \phi_F + a_B \phi_B$$

$b = S_p \Delta v$, $c = S_u \Delta v$

in which Sp and Su are coefficients in the source terms determined from a suitable finite difference approximation of (Sϕ) expression for particular dependent variable ϕ.

Solving this using upwind scheme to give values of a$_i$

$$\left. \begin{array}{l} a_E = D_e + \langle 0, F_e \rangle; a_W = D_w + \langle F_W, 0 \rangle; a_N = D_n + \langle 0, -F_n \rangle \\ a_S = D_s + \langle F_s . 0 \rangle; a_F = D_f + \langle -F_f . 0 \rangle; a_B = D_b + \langle 0, F_b \rangle \end{array} \right\} \qquad (16)$$

The convection and diffusion fluxes are given by :

$$\left. \begin{array}{l} F_e = (\rho U)_e \Delta y \Delta z \ \& \ D_e = \Gamma_e \Delta y \Delta z / \delta x_e \ \& \ F_w = (\rho U)_w \Delta y \Delta z \ \& \ D_w = \Gamma_w \Delta y \Delta z / \delta x_w \\ F_n = (\rho V)_n \Delta x \Delta z \ \& \ D_n = \Gamma_n \Delta x \Delta z / \delta y_n \ \& \ F_s = (\rho V)_s \Delta x \Delta z \ \& \ D_s = \Gamma_s \Delta x \Delta z / \delta y_s \\ F_f = (\rho W)_f \Delta x \Delta y \ \& \ D_f = \Gamma_f \Delta x \Delta y / \delta z_f \ \& \ F_b = (\rho W)_b \Delta x \Delta y D_b = \Gamma_b \Delta x \Delta y / \delta z_b \end{array} \right\} (17)$$

All the coefficients in Eq.(16) and (17) are used for solving of (k and ε), the velocity components are calculated on a staggered grid and their values differ.

Excluded the pressure terms from the coefficient of the source terms Su, the discretized equation for (U_e , V_n , W_f) are

$$\left. \begin{array}{l} a_e U_e = \sum_i a_i U_i \ + c + (P_P - P_E)\Delta y \Delta z \\ a_n V_n = \sum_i a_i V_i \ + c + (P_P - P_N)\Delta x \Delta z \\ a_f W_f = \sum_i a_i W_i \ + c + (P_P - P_F)\Delta x \Delta y \end{array} \right\} \qquad (18)$$

The velocities in Equations (18) will all satisfy continuity if the pressures at the grid points are correct. At the start of the calculation, only guessed values of pressure and velocity are available and continuity will not be satisfied. Therefore, some means of correcting the pressures is needed to achieve a solution. Using SIMPLE procedure [Onbasiogla and Husegin (2003)]. The SIMPLE assume that,

K. A. H. Ismael	Numerical and Experimental Investigation on the
I.M. Fayed	Effect of Restriction Shape on Characteristics of
H.A. Hadi	**Airflow in a Square Duct**

$$P = P^* + P' ; U = U^* + U' ; V = V^* + V' ; W = W^* + W' \Big\} \tag{19}$$

where the asterisk represents a guessed value and the prime is the correction necessary to satisfy continuity.

$$\left.\begin{aligned}
a_e U_e^* &= \sum_i a_i U_i^* + c + (P_P^* - P_E^*)\Delta y \Delta z \\
a_n V_n^* &= \sum_i a_i V_i^* + c + (P_P^* - P_N^*)\Delta x \Delta z \\
a_f W_f^* &= \sum_i a_i W_i^* + c + (P_P^* - P_F^*)\Delta x \Delta y
\end{aligned}\right\} \tag{20}$$

Subtracting equations (18) from equations (20) we get:

$$\left.\begin{aligned}
a_e U_e' &= \sum_i a_i U_i' + (P_P' - P_E')\Delta y \Delta z \\
a_n V_n' &= \sum_i a_i V_i' + (P_P' - P_N')\Delta x \Delta z \\
a_f W_f' &= \sum_i a_i W_i' + (P_P' - P_F')\Delta x \Delta y
\end{aligned}\right\} \tag{21}$$

For computational convenience, $\sum_i a_i U_i'$, $\sum_i a_i V_i'$, and $\sum_i a_i W_i'$ are set to zero[Onbasiogla and Husegin (2003)]. Substituting the result of eq.(19) with eq.(21) into continuity equation get:

$$\sum_i a_i P_P' = \sum_i a_i P_i' + c \tag{22}$$

where $\sum_i a_i = a_E + a_W + a_N + a_S + a_F + a_B$

$$\sum_i a_i P_P' = a_E P_E' + a_W P_W' + a_N P_N' + a_S P_S' + a_F P_F' + a_B P_B'$$

$a_E = (\rho_e/a_e)(\Delta y \Delta z)^2$ & $a_W = (\rho_w/a_w)(\Delta y \Delta z)^2$ & $a_N = (\rho_n/a_n)(\Delta x \Delta z)^2$ &

$a_S = (\rho_s/a_s)(\Delta x \Delta z)^2$ & $a_F = (\rho_f/a_f)(\Delta x \Delta y)^2$ & $a_B = (\rho_b/a_b)(\Delta x \Delta y)^2$

$$c = F_w^* - F_e^* + F_s^* - F_n^* + F_f^* - F_b^*$$

$F_w^* = (\rho U^*)_w \Delta y \Delta z$ & $F_e^* = (\rho U^*)_e \Delta y \Delta z$ & $F_s^* = (\rho V^*)_s \Delta X \Delta z$ &

$F_n^* = (\rho V^*)_n \Delta x \Delta z$ & $F_b^* = (\rho W^*)_b \Delta x \Delta y$ & $F_f^* = (\rho W^*)_f \Delta x \Delta y$

Under relaxation is implemented to a void divergence in the solution variable. The under relaxation factor used in this study is (0.5) for U, V, W, k & ε and (0.8) for P .

RESULTS AND DISCUSSION:
Experimental Results:
Pressure Drop Investigation:

The total pressure drop (ΔP_T) through the duct with restriction can be broken down into two components which are pressure drop due to the friction (ΔP_f) and the inertia losses through the restriction (ΔP_R)

$$\Delta P_T = \Delta P_f + \Delta P_R$$

Pressure Drop Due to the Restriction Geometry ΔP_R:

Fig.(4) shows a typical pressure drop pattern along the duct (with different restriction shapes and different Reynolds numbers). It contains 13 restriction shapes, each restriction has four graphs for different Reynolds numbers.

It is clear that the pressure drop data fall on a straight line in the upstream section, and that near the restriction there is substantial pressure depression. However, the pressure depression is recovered along the downstream data and fall on a straight line again. Without the restriction, the two straight lines would be collinear. Thus the

pressure drop due to the different restriction shape (ΔP_R) is the difference offset by the two lines (between (A) and (B)). The pressure drop component (ΔP_R) can be expressed by

$$\Delta P_R = \frac{1}{2}\rho_{air}U_{av}^2 \cdot k_R$$

where the k_R: pressure coefficient due to the restriction.

The pressure coefficient (k_R) is due to the inertia losses, so it is independent of Reynolds number [Lee (1986)]. This can be seen in Fig. (5), this figure is plotted between pressure coefficient k_R vs the Reynolds numbers for four shapes and different blockage area ratio of restrictions which are used in this work. It is clear that the values of k_R are roughly constant with the range of Reynolds number which is used for the same restriction [Roberson and Crowe (1977)] .The behaviors of k_R for the other restrictions are in line with the four restrictions which are drawn. The parameters that k_R depends on are: the ratio between the wetted perimeter of the restriction to the free remainder perimeter (p_e/P_e), and the blockage area ratio A_b. Table (2) shows the wetted perimeter and the blockage area ratio for all restrictions which are used in this study.

Table (2) Wetted perimeter and blockage area ratio for all Restriction shapes

Restriction	Blockage area ratio A_b	Wetted perimeter p_e cm	Remainder perimeter P_e cm	p_e/P_e	Average k_R
	0.11	8	40	0.2	0.6
	0.11	12	36	0.53	0.62
	0.11	16	32	0.5	0.65
	0.22	16	32	0.5	0.72
	0.22	12	36	0.33	0.69
	0.22	20	28	0.7	0.74
	0.33	24	24	1	0.75
	0.33	20	28	0.7	0.72
	0.33	24	24	1	0.76
	0.33	12	36	0.33	0.69
	0.44	16	32	0.5	0.79
	0.44	20	28	0.7	0.82
	0.56	24	24	1	0.83

Correlation between k_R , p_e/P_e and A_b :

To create the relation between k_R and the two parameters (p_e/P_e) and A_b assume the general formula between them: $k_R = a.(\frac{p_e}{P_e})^b.A_b^c$

where: a , b and c are correlation constant .

K. A. H. Ismael	Numerical and Experimental Investigation on the
I.M. Fayed	Effect of Restriction Shape on Characteristics of
H.A. Hadi	Airflow in a Square Duct

To solve this relation, use statistical program which uses Quais-Newtons method to obtain

$$k_R = 0.881(\frac{P_e}{P_e})^{0.064}.A_b^{0.123}$$

and with accuracy of 96% as shown in Fig.(6). It is clear from the correlation equation mentioned above that the effect of the blockage area ratio A_b on k_R is much greater, if the ratio of perimeter is kept constant.

Pressure Drop Due to The Friction ΔP_f :

Fig.(7) is drawn between C_f Vs (z/D_h). In general, as shown in the figure, for all restrictions which are used in the study, the friction factor C_f is a function of Reynolds number. Each restriction uses the relations between C_f and Reynolds number are roughly have same behavior for different Reynolds numbers , but the values of C_f decrease with decreasing of Reynolds number.

The maximum values of C_f in the downstream region after restriction as they appear in the (z/D_h) equal $(1/3)$ or in the distance (4 cm) from restriction in z-direction, except the restrictions number $(3,10,11,\&12)$ the maximum C_f appears in the (z/D_h) equal to $(2/3)$ or in the distance (8 cm) from restriction in z-direction.

Total Pressures Coefficients:

The total pressures coefficients after restriction are presented in Fig. (8) for $Re_1=8.2\text{x}10^4$ and $Re_4=5.6\text{x}10^4$. The Cp_T contours for the same restriction seem to be approximately similar in behavior and have different values with the changing of Reynolds number. When Reynolds number decreases the Cp_T decreases, this explains why the losses decrease when Reynolds number decreases.

It is clear from the figure that the values of Cp_T are positive in the area behind the restriction (positive pressure area), and they are negative in remainder area (suction area), for all restrictions which are used in this study.This distribution depends on the blockage area ratios as shown in Fig. (8). To explain this effect take for example of blockage areas (0.11) and (0.56), the blockage area ratio increases (80%), the value of Cp_T increases around (83%) (i.e. the losses are increased). The main conclusion is that, when the blockage area ratio increases the Cp_T increases also so that the losses increase.

Axial Velocity Distribution:

The axial velocity Distribution for selected three restriction shapes No.(3,9&13) at $Re_1=8.2\text{x}10^4$ are presented in Fig.(9). Restriction No.(3,9&13) represent three different blockage area ratios of $(0.11,0.33$ and $0.56)$ respectively. This figure is drawn for axial velocity with y-direction in four positions (2, 4, 8 & 12 cm) in z-direction. In each location there are three graphs for different distances in x-direction (3, 6 & 9 cm), these positions represent the points of measurements in z-direction by five-hole probe.

It is clear from the figure mentioned above that for all restrictions the velocity behind the restriction has the lowest value approximately reaching zero, but the values in open area are greater than the main flow velocity.

NUMERICAL RESULTS:
Flow Patterns (Streamlines and Velocity Vectors) :

Streamlines and velocity vectors are plotted in z-x plane at y=6 cm as shown in Fig.(10) (a and b) for three restriction at two Reynolds number.

So far considered flow in which the pressure outside the boundary layer was considered as constant. If, however, the pressure varies in the direction of flow (because of the restriction), the behavior of the fluid may be greatly affected [Massey]. Fig.(10) shows that the streamlines in the upstream region are parallel and the velocity vectors distributions are symmetric in any location, when the flow strikes the restriction (normal to the flow direction), the streamlines approach one another in the open area and large eddies directly form after the restriction, their strength depend on the Reynolds number and the restriction shape and position. The velocity vectors behind the restriction have the lowest values approach to zero and have the highest values in the open area.

Axial Velocity Distribution:

Fig.(11) represents the axial velocity distribution for three selected restriction No.(3,9,13) with different blockage area ratio at $Re_1=8.2 \times 10^4$.

This figure is drawn for axial velocity with y-direction in four positions (2, 4, 8 and 12 cm) in z-direction. In each position there are three graphs for different distances in x-direction (3, 6 & 9 cm), these positions represent the same points of measurement in experimental work.

It is clear from the figure mentioned above that the velocity profiles at x=3 cm and x=9 cm are the same for all z (due to the symmetry of all restrictions used) and the velocity behind the restriction has the lowest values (at x=6 cm), but the values of velocity in the open area are greater than the main flow velocity. The velocity distribution in both cases (theoretically and experimentally) is equintativly the same but there are slightly difference in velocity values for all cases studied.

CONCLUSION:
From Experimental Work

- The pressure drop coefficient due to the restriction shape and position, (k_R) is independent of the Reynolds number in study range but it depends on the blockage area ratio (A_b) and the ratio between the wetted perimeter and free remainder perimeter (p_e/P_e). Correlation equation is created between them.

$$k_R = 0.881(\frac{pe}{Pe})^{0.064}.A_b^{0.123}$$

- The total pressure coefficient C_{Pt} decreases when the Reynolds number decreases for same restriction, and it depends on the blockage area ratio, when the blockage area ratio increases around 80% the C_{Pt} increases approximately 83%.

- The axial velocity U has the lowest value behind restriction approach to zero, but the values in open area are greater than those of the main flow velocity. This conclusion is in line with the numerical and Fluent (6.1) results

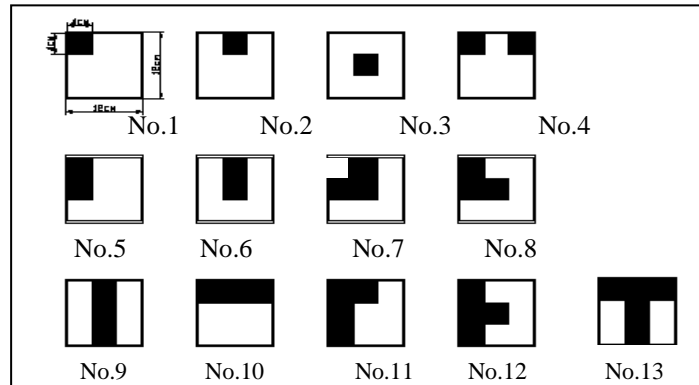| K. A. H. Ismael | Numerical and Experimental Investigation on the |
| I.M. Fayed | Effect of Restriction Shape on Characteristics of |
| H.A. Hadi | Airflow in a Square Duct |

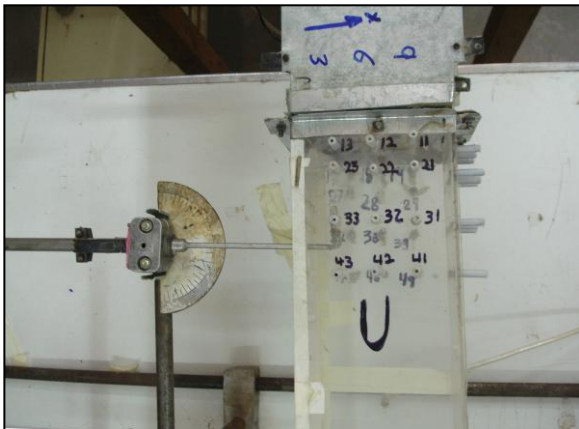Figure (1) The restrictions shapes.

Figure (2a) Photograph shows the static pressure taps.
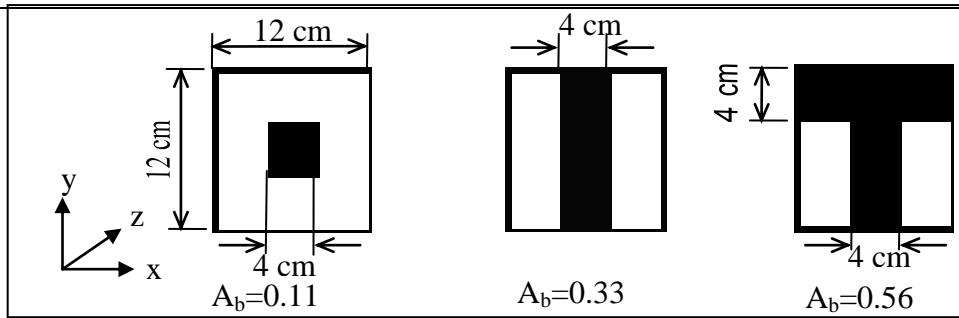

Figure (2b) Photograph of the air supply and test rig
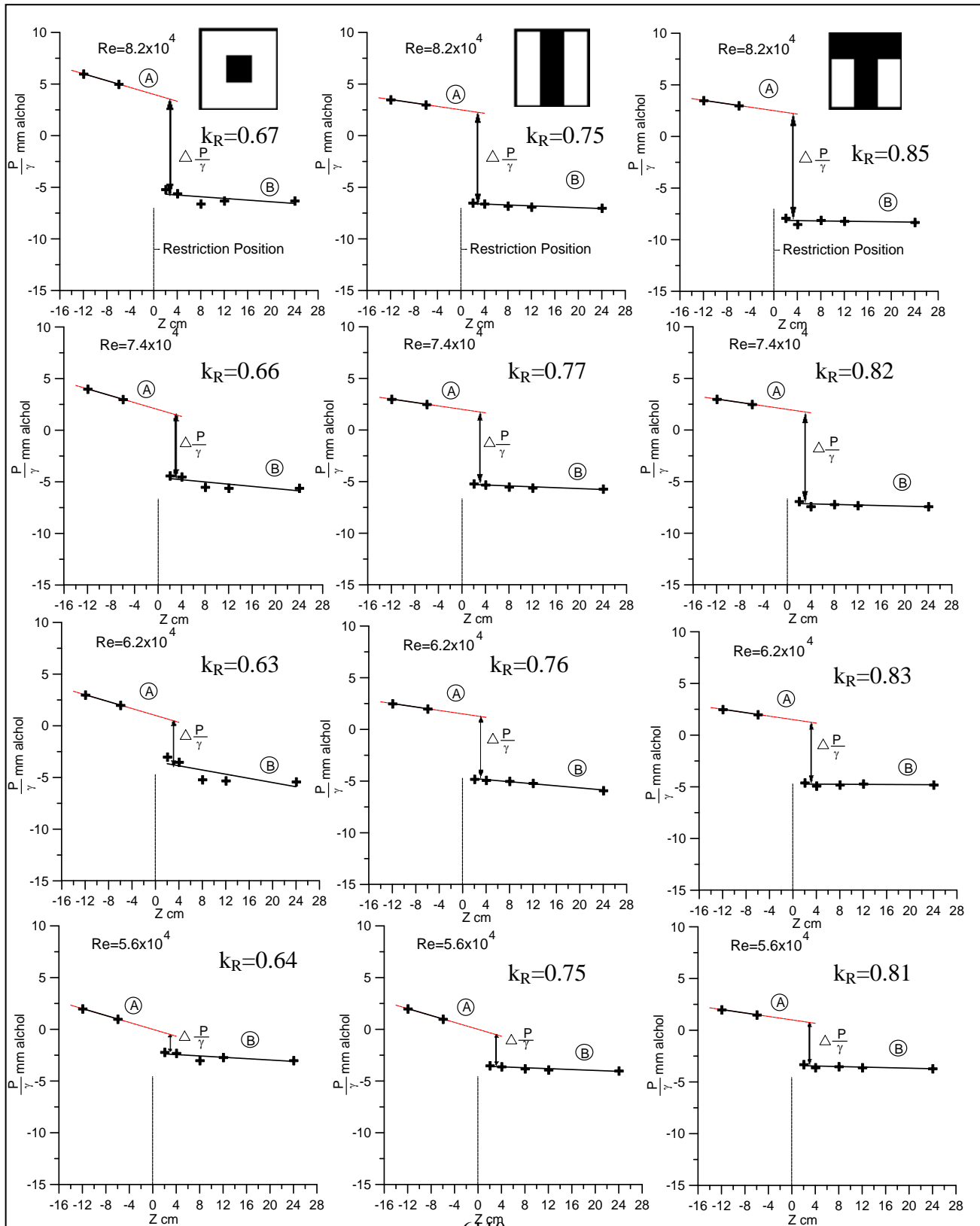
Figure (3) The restriction models

Figure (4) Pressure drop induct with restriction for different Reynolds numbers,
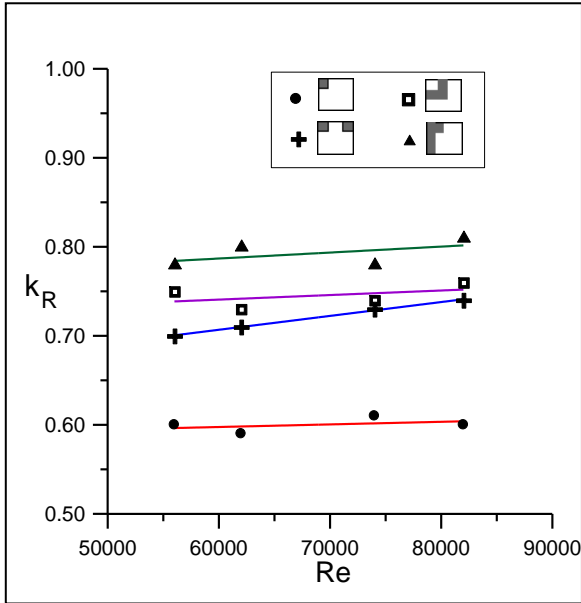$Re_1= 8.2\times10^4$, $Re_2=7.4$, $Re_3=6.2\times10^4$ & $Re_4=5.6\times10^4$.

K. A. H. Ismael
I.M. Fayed
H.A. Hadi

Numerical and Experimental Investigation on the
Effect of Restriction Shape on Characteristics of
Airflow in a Square Duct

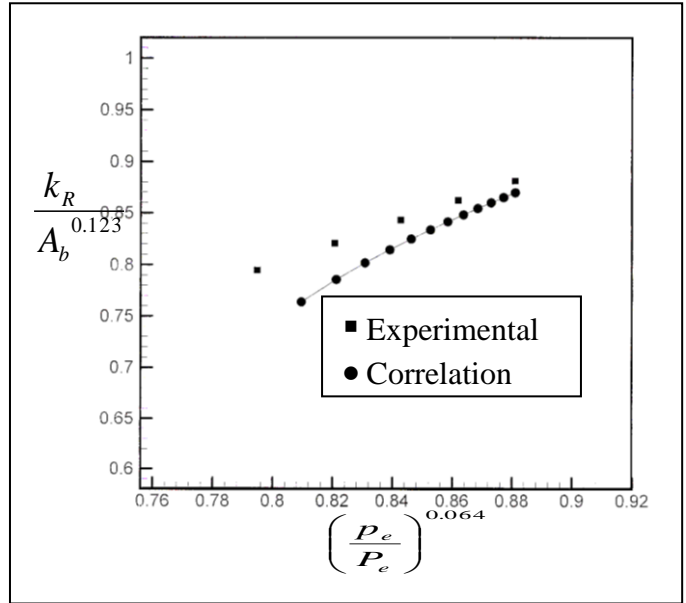Figure (5) Pressure coefficient Vs Reynolds numbers for different shape.

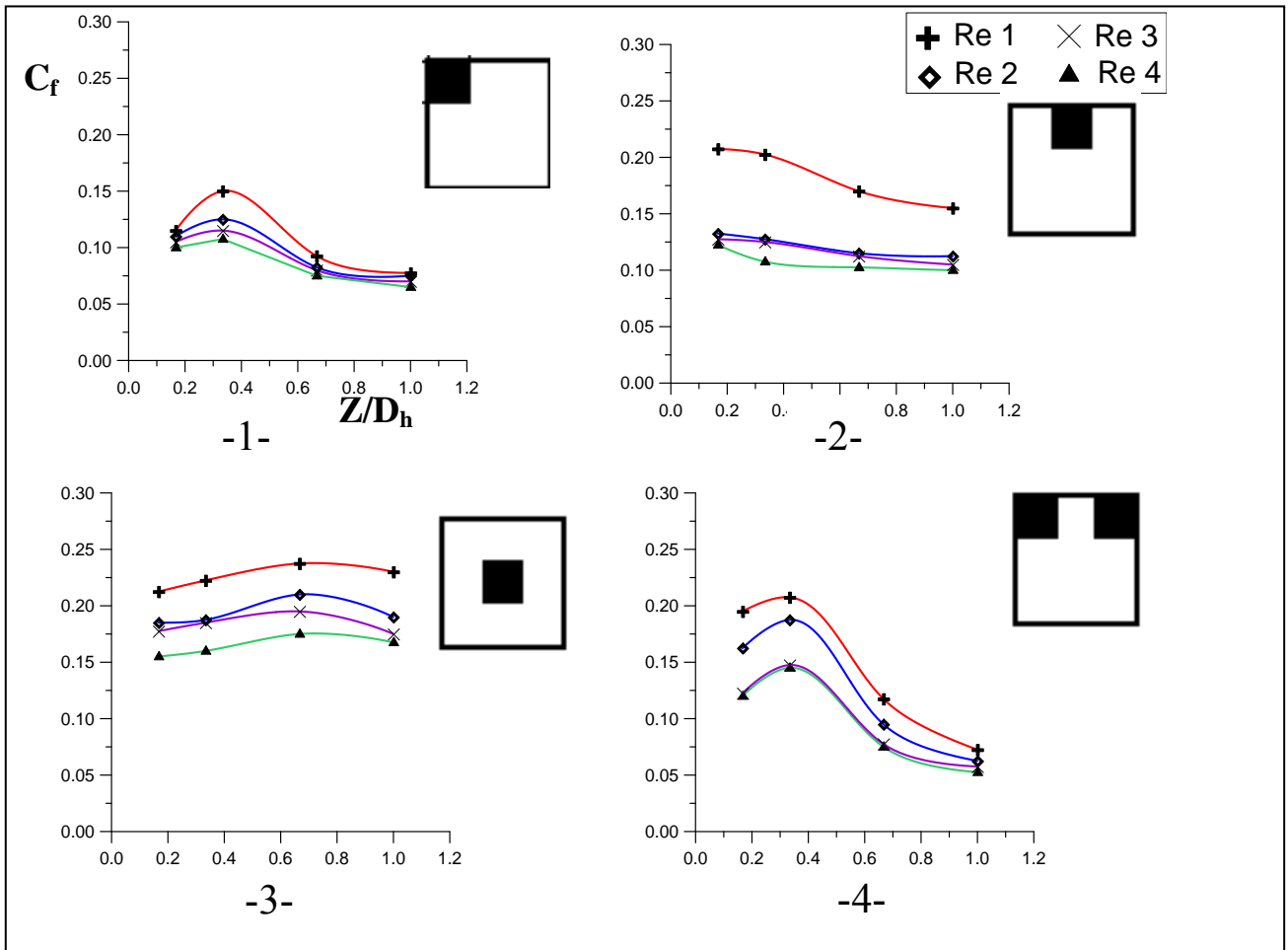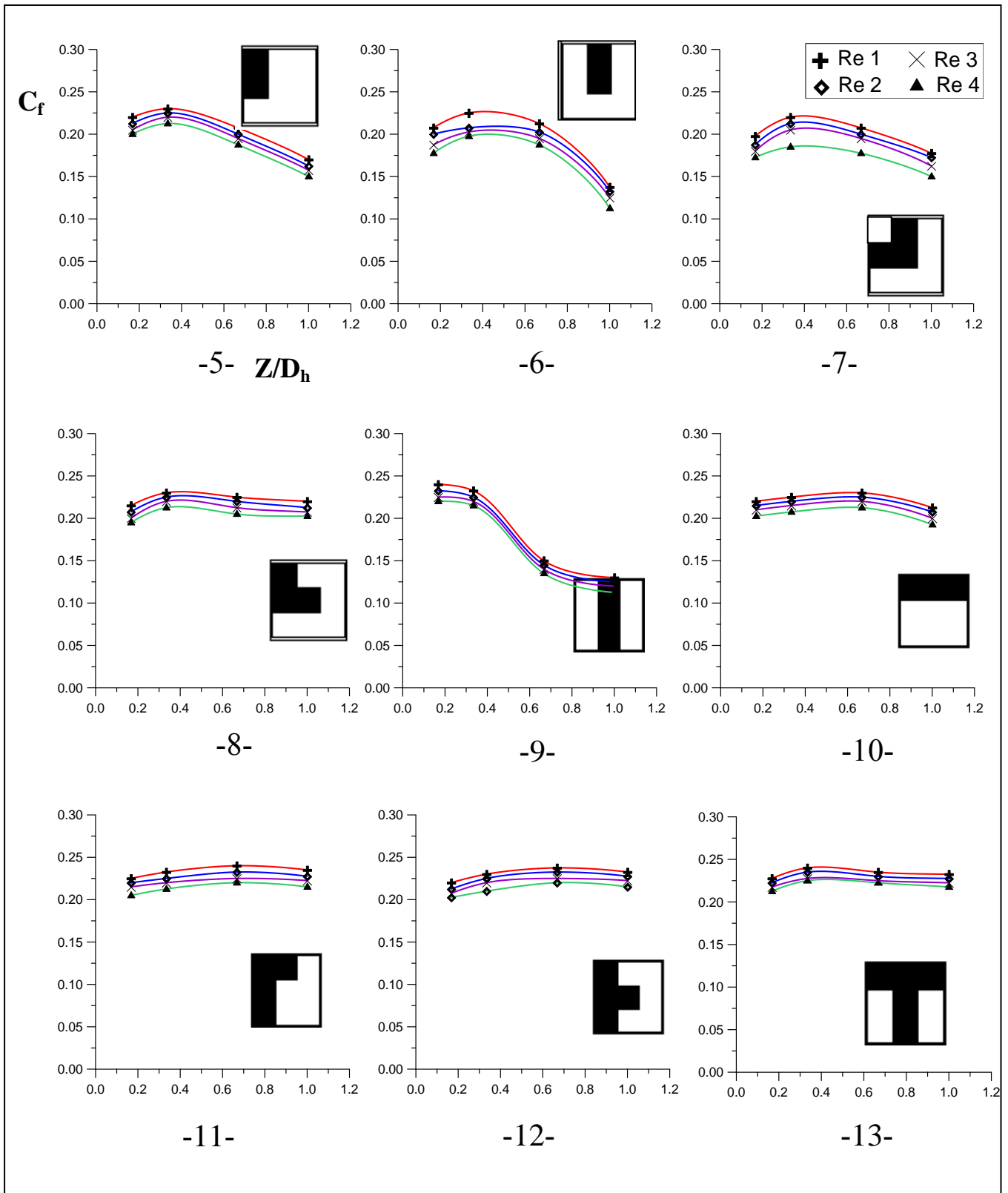Figure (6) Correlation between pressure coefficient k_R and perimeter ratio p_e/P_e and Blockage area ratio A_b.

Figure (7) The effect of restriction position on the C_f for different Reynolds numbers, $Re_1= 8.2 \times 10^4$, $Re_2=7.4 \times 10^4$, $Re_3=6.2 \times 10^4$ & $Re_4=5.6 \times 10^4$.

Continued to figure (7)

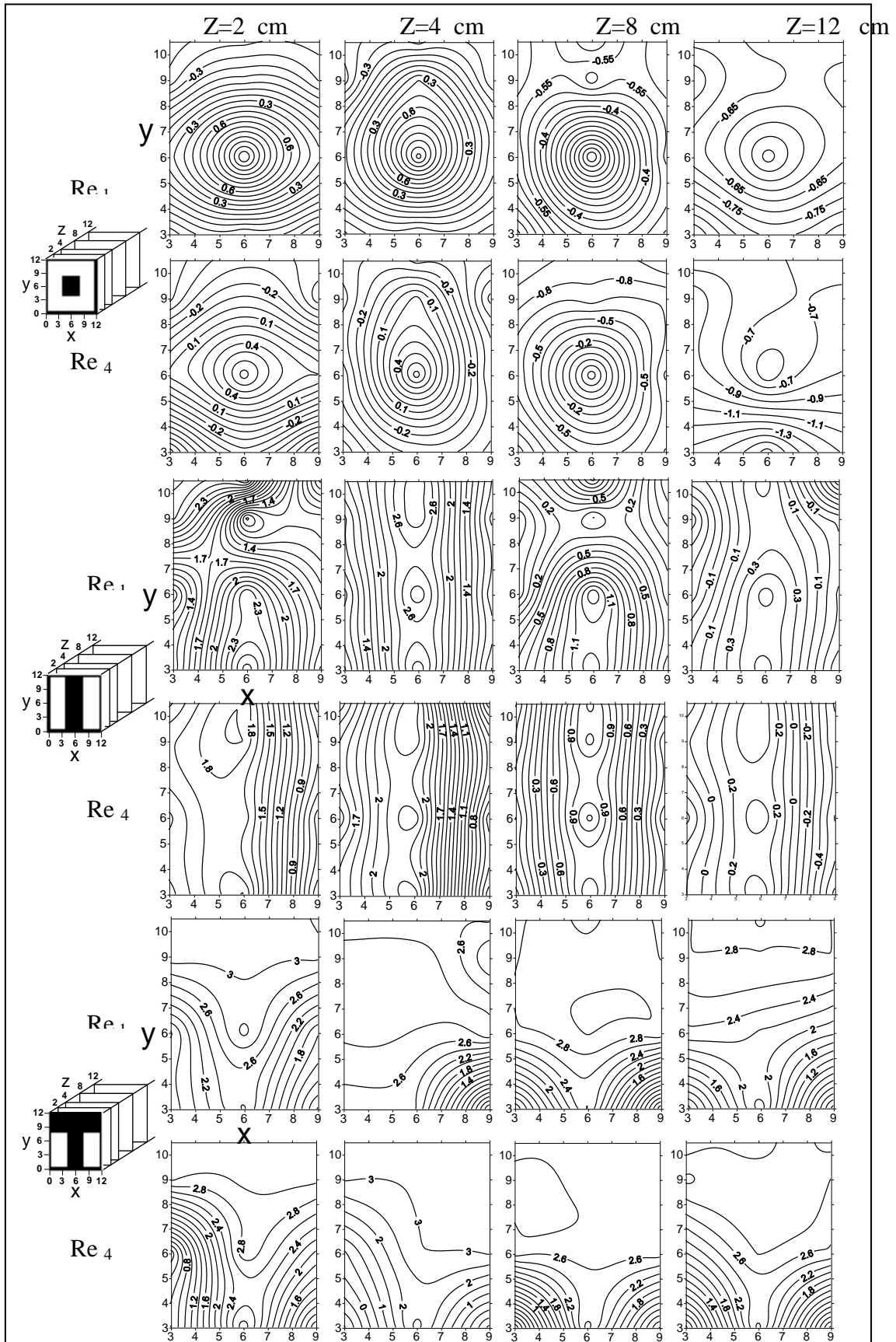| K. A. H. Ismael | Numerical and Experimental Investigation on the |
| I.M. Fayed | Effect of Restriction Shape on Characteristics of |
| H.A. Hadi | **Airflow in a Square Duct** |

Figure (8) Variation of Total Pressure Coefficient Cp_T for different section at $Re_1=8.2 \times 10^4$ & $Re_4=5.6 \times 10^4$.

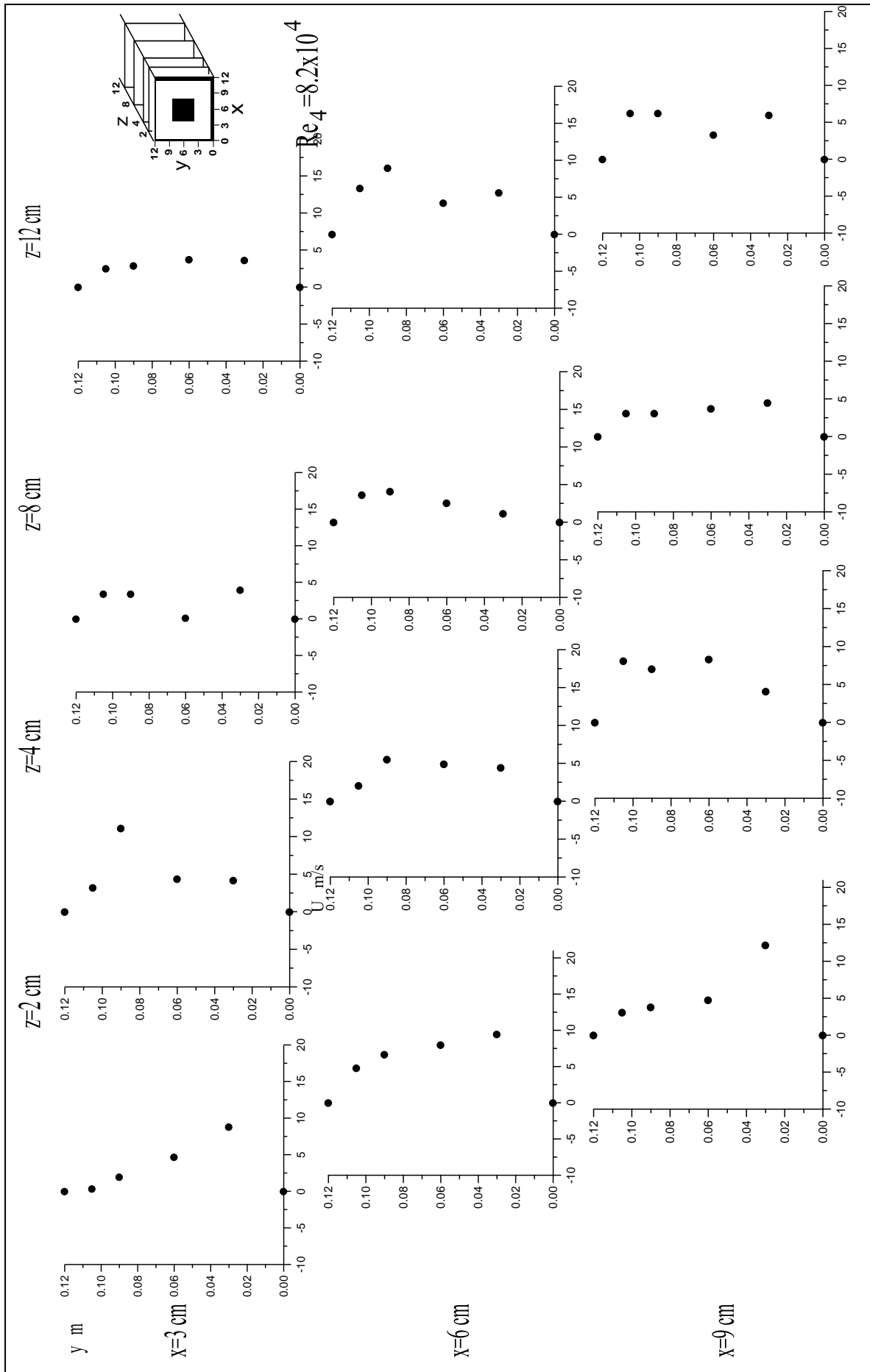Figure (9) Axial velocity distrbution for different section in experimintal work

K. A. H. Ismael
I.M. Fayed
H.A. Hadi

Numerical and Experimental Investigation on the
Effect of Restriction Shape on Characteristics of
Airflow in a Square Duct

Continued to Figure (9)

$Re_4 = 8.2 \times 10^4$

z=2 cm   z=4 cm   z=8 cm   z=12 cm

y m

x=3 cm

U m/s

x=6 cm

x=9 cm

Continued to Figure (9)

K. A. H. Ismael
I.M. Fayed
H.A. Hadi

Numerical and Experimental Investigation on the
Effect of Restriction Shape on Characteristics of
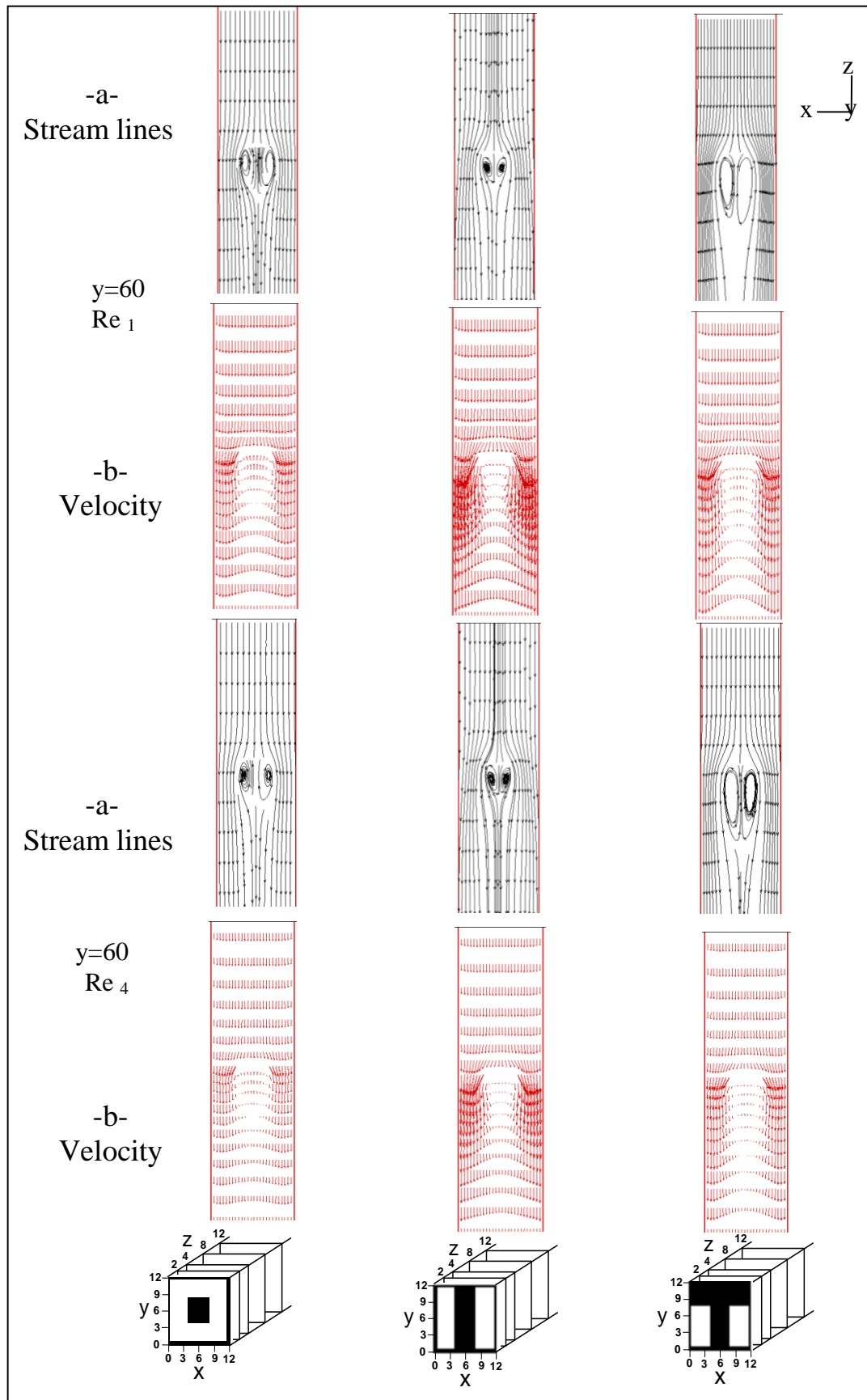**Airflow in a Square Duct**
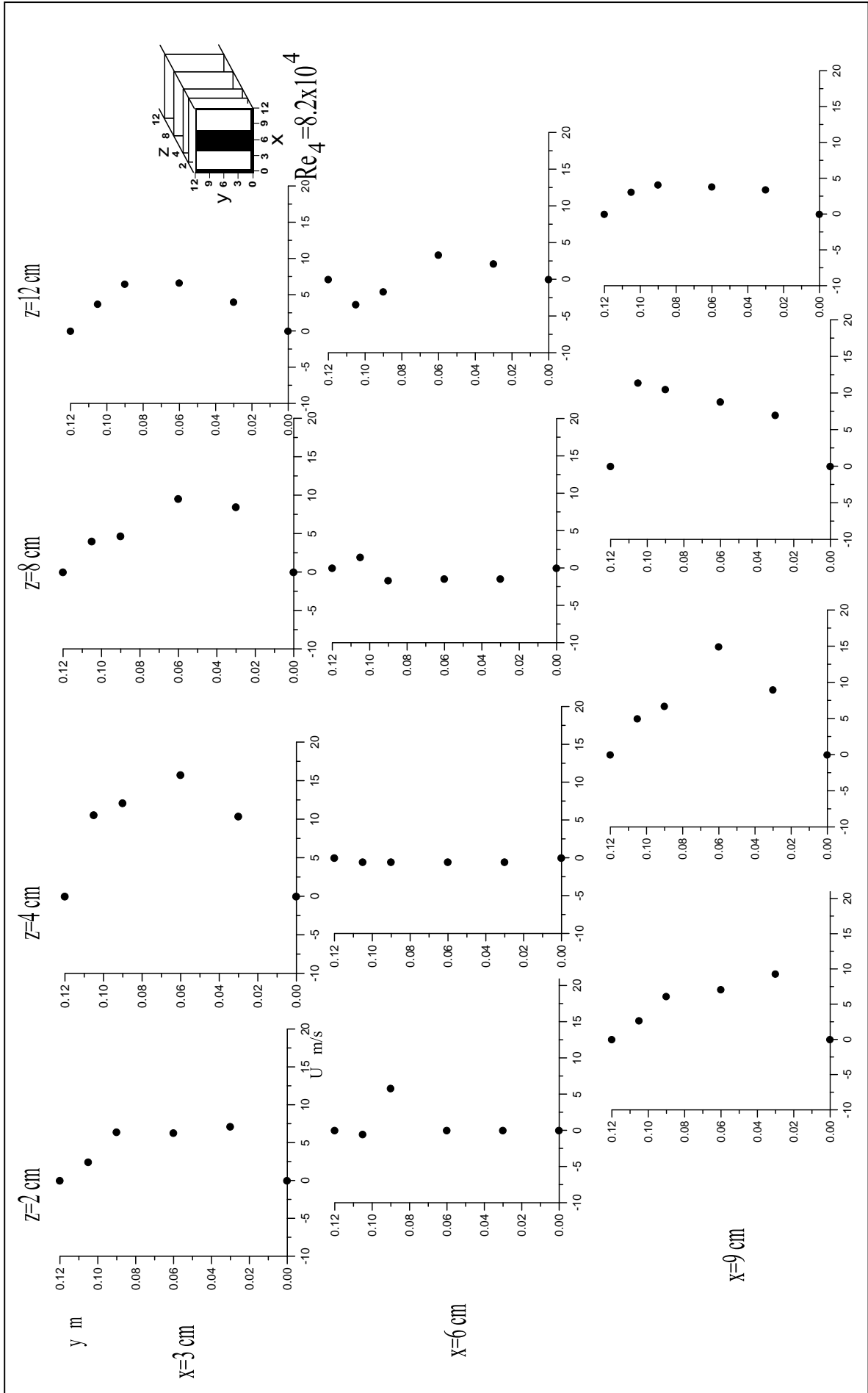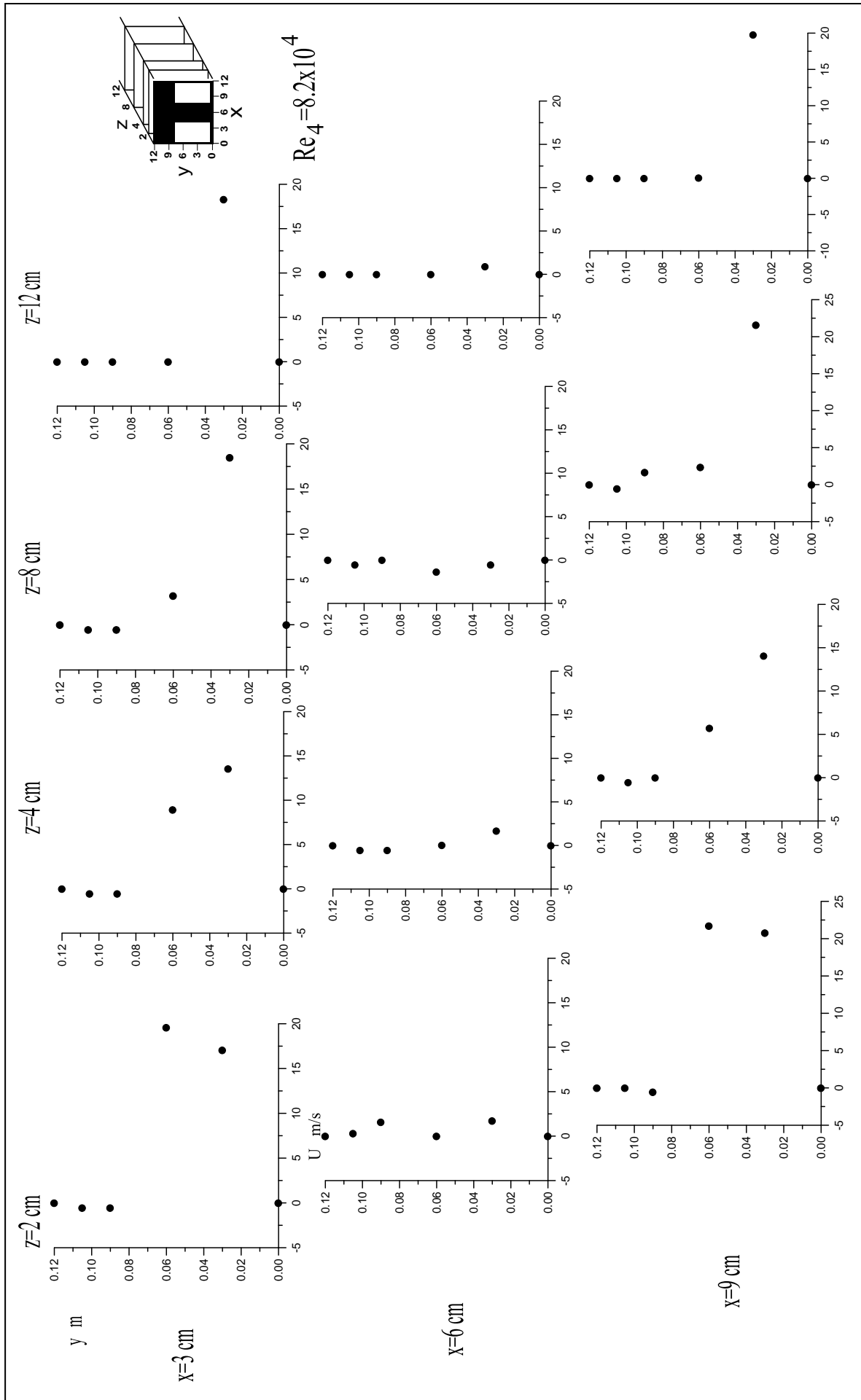
Figure (10) Flow patterns in z-x plane at $Re_1=8.2 \times 10^4$ & $Re_4=5.6 \times 10^4$
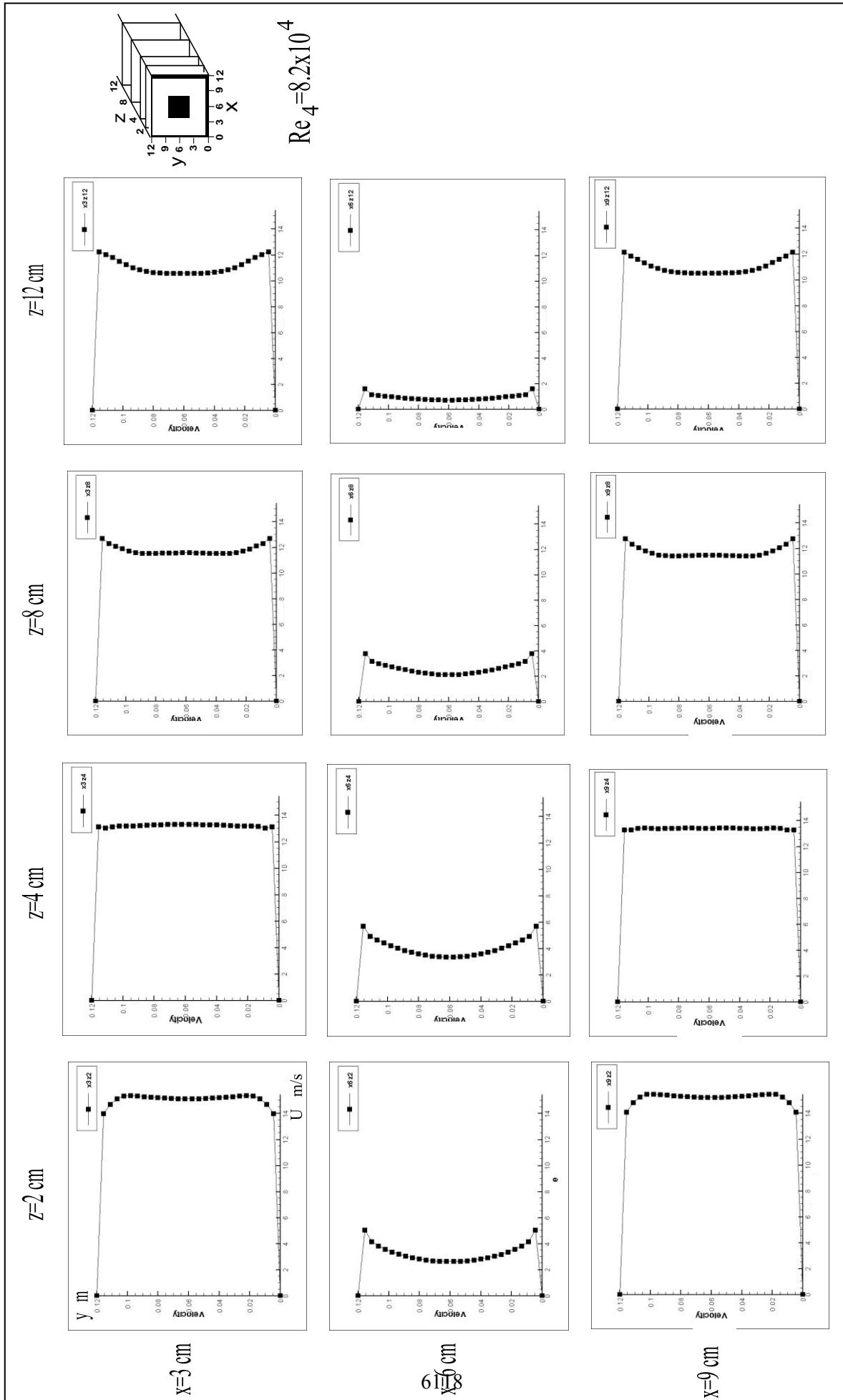
Figure (11) Axial velocity distrubution for different section in numerical work.

K. A. H. Ismael
I.M. Fayed
H.A. Hadi

**Numerical and Experimental Investigation on the
Effect of Restriction Shape on Characteristics of
Airflow in a Square Duct**
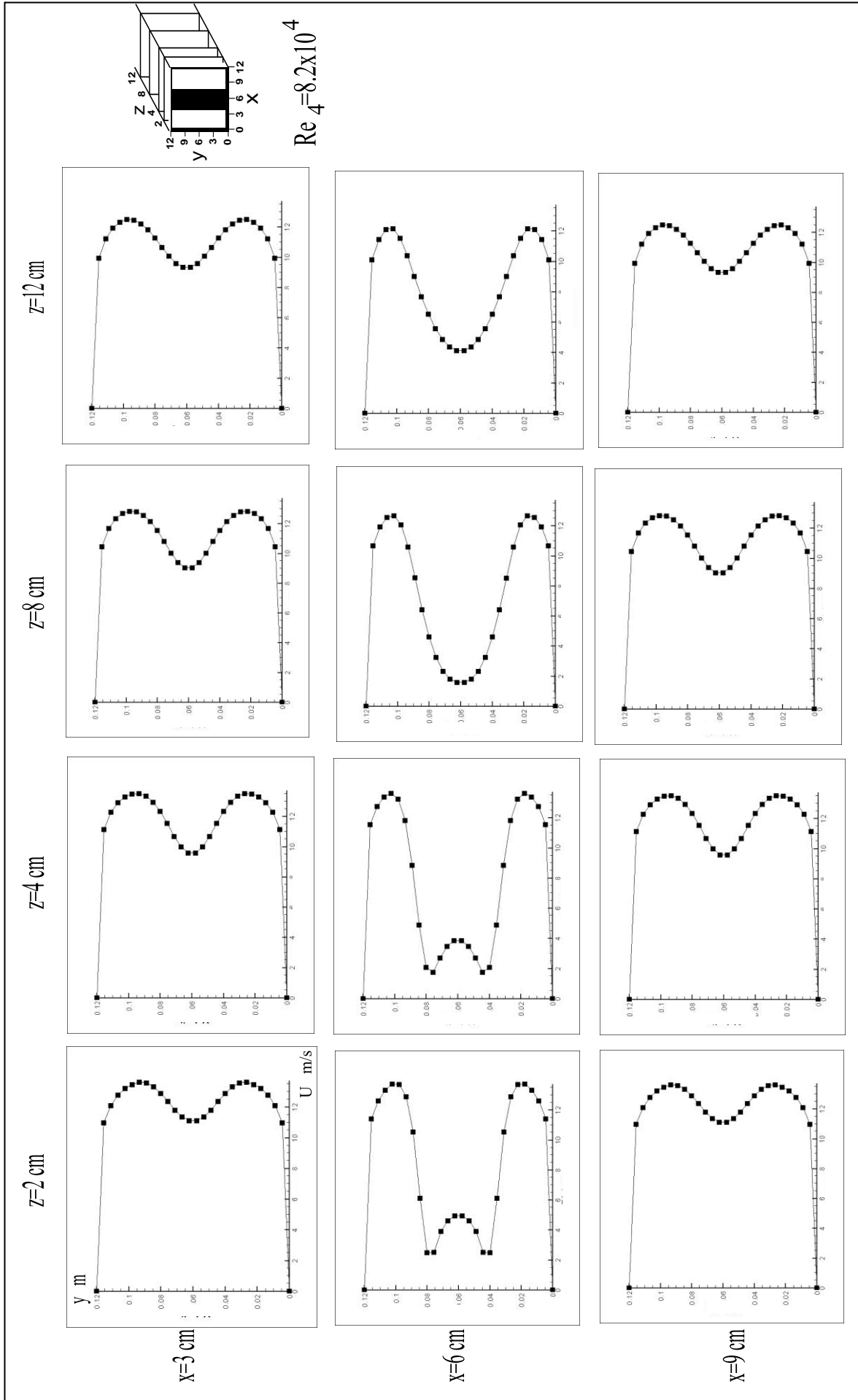
Continued to Figure (11)

Continued to Figure (11)

K. A. H. Ismael	Numerical and Experimental Investigation on the
I.M. Fayed	Effect of Restriction Shape on Characteristics of
H.A. Hadi	**Airflow in a Square Duct**
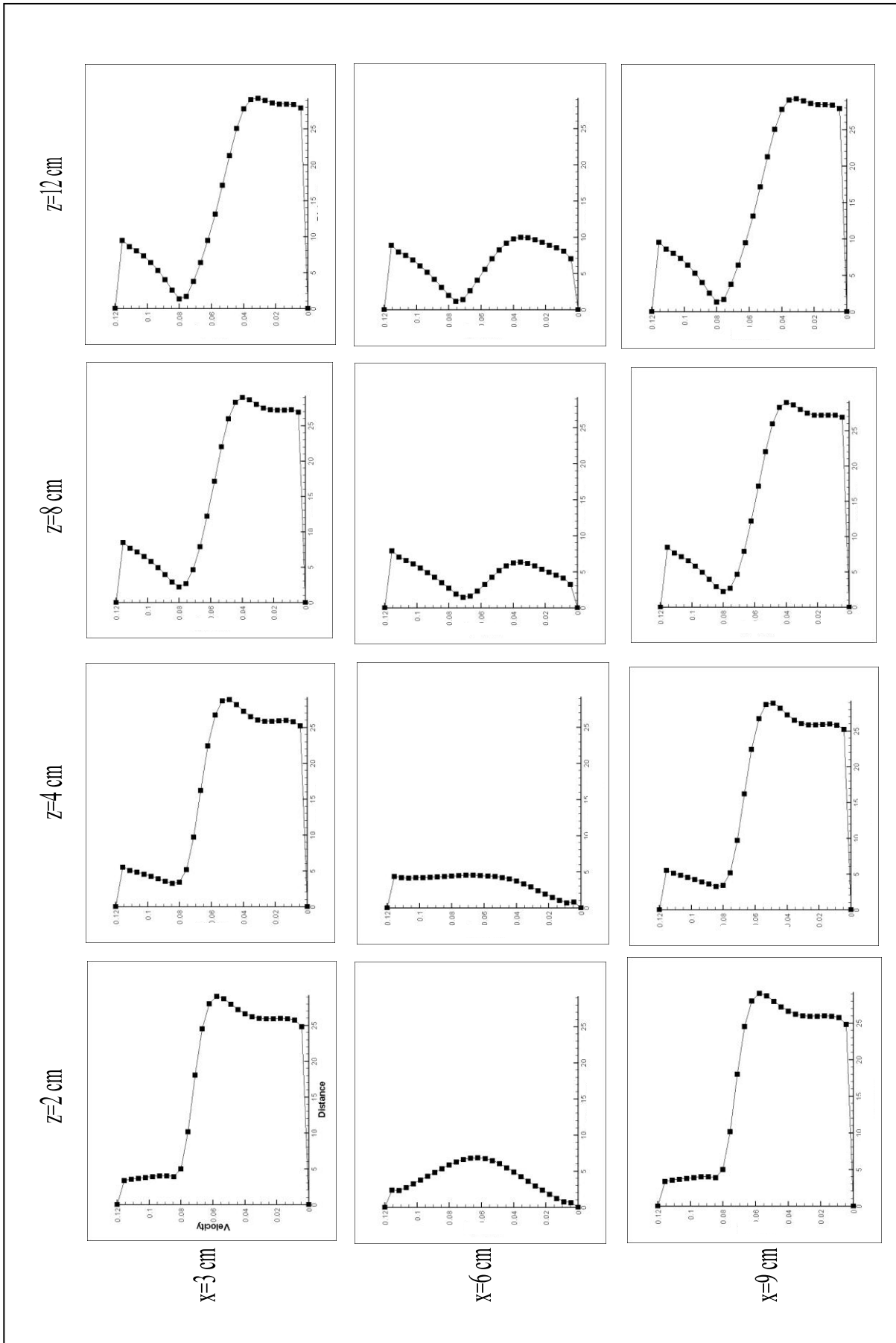
REFERENCES

- British-standard 1042, "Method for measurement of fluid flow in pipes", Part 2A, August, 1973.
- Davidson, L., and Farhanieh, B., "A finite volume code employing collocated variable arrangement and Cartesian velocity components for computational geometries.", Dep. Of Thermo and Fluid Dynamics, Chalmers University of Technology, Sweden, November, 1995, Publ. No. 95/11.
- Han, J.C., Glicjsman, L.R., and Rohsenow, W.M.,(1978),"An investigation of heat transfer and friction for rib-roughened surfaces. ", Int. J., Heat and Mass Transfer Vol. 21, pp. 1143-1156.
- Hanaa Abdul hadi" Numerical and Experimental Investigation on the Effect of Restriction Shape on Characteristics of Airflow in a Square Duct." Ph.D thesis of Mechanical Engineering of University of Technology,2006.
- Han,J.C.,(1984),"Heat transfer and friction in channels with two opposite rib-roughened walls. ", Transaction of the ASME, Vol. 106, Nov. 1984.
- Launder, B.T., and Spalding, D.B., "Lecturers in mathematical models of turbulence.' Department of Mechanical Engineering, imperial college of Science and Technology, London, England.
- Lee, Y.N., (1986), "Heat transfer and pressure drop characteristics of an array of plates aligned at angles to the flow in a rectangular duct. ", Int. J., Heat and Mass Transfer Vol. 29, No. 10, pp. 1553-1563, 1986.
- Massey B.S., "Mechanics of Fluids", 4th edition, Van Nostr and Reinhold, 1980.
- Ooi , A. , Iaccarino , G., Durbin , P.A. , and Behnia , M. , (2002). " Reynolds averaged simulation of flow and heat transfer in ribbed ducts. ", International Journal of Heat and Fluid Flow, Vol. 23 , (2002) , pp. 750-757.
- Ooi, A., Iaccarino, G., Durbin, P.A., and Behnia, M., (2003). "Simulation of turbulent flow and heat transfer in complex passage. ", Journal of Heat and Fluid Flow , Vol. 23 , pp. 750-757.
- Onbasioglu, S.U., and Huseyin Oube, H., (2003),"On enhancement of heat transfer with ribs.", Applied Thermal Engineering, Vol. 24, Issue 1, January 2004, pp. 43-57.
- Patanker, S.V., (1980), "Numerical heat transfer and fluid flow ", McGraw.Hill, New York.
- Roberson and Crowe, "Engineering Fluid Mechanics." 6th edition, Copyright 1977, by John Wilely and Sons, Inc.
- Taslim, M.E., Li, T., and Spring, S.D., (1998)," Measurement heat transfer coefficients and friction factor in passage rib-roughened on all walls", Transactions of ASME, Vol. 120, July, 1998.

LIST OF SYMBOLS

Symbol	Title	Units
A_b	Blockage area ratio	m^2
$a_E, a_W, a_N, a_S, a_F, a_B$	Coefficient in turbulence model	---
C_f	Pressure coefficient due to the friction	---
$C_\mu, C_{1\varepsilon}, C_{2\varepsilon}$	Constant in turbulence model	---
G_k	Generation rate or turbulence energy	---
i,j,k	Indices which indicate position in (x,y,z)	---
k_R	Pressure coefficient due to the restriction	---
P_{av}	Average pressure	N/m^2
p_e	Wetted perimeter	m
P_e	Remainder perimeter	m
P_s	Static pressure	N/m^2
U, V, W	Mean velocities in x,y,z directions	m/s
U_{av}	Average velocity	m/s
ε	Energy dissipation	m^2/sec^3
μ	Dynamic viscosity	$N/sec. \, m^2$
ν	Kinematics viscosity	m^2/sec
ϕ	Dependent variables	---
e, w, n, s, l, r Subscript	Control volume faces	----